J. Chem. Thermodynamics 161 (2021) 106516

Contents lists available at ScienceDirect

J. Chem. Thermodynamics

journal homepage: www.elsevier.com/locate/jct

# Heat of mixing profile, complexation curve and spectroscopic investigation of binary mixtures containing bicyclic Brønsted superbase DBN with hydrogen ethanoate

Gordon W. Driver [a,*], L.M.J. Sprakel [b,c], Ilkka Kilpeläinen [a], Boelo Schuur [b]

[a] Materials Chemistry Division, Department of Chemistry, Faculty of Science, P.O. Box 55 (A.I. Virtasen aukio 1), FI-00014 University of Helsinki, Finland
[b] Sustainable Process Technology Group, Faculty of Science and Technology, University of Twente, Meander Building 221, De Horst 2, 7522 LW Enschede, the Netherlands
[c] BBOne Technology & Investments, Wilgenhaege B.V., Marktplein 47, 2132 DA Hoofddorp, the Netherlands

ARTICLE INFO

*Article history:*
Received 2 December 2020
Received in revised form 4 May 2021
Accepted 5 May 2021
Available online 08 May 2021

*Keywords:*
Superbase
Heat of mixing
Ionic liquids
Isothermal titration calorimetry
Complexometric titration
Double liquid salt

ABSTRACT

Isothermal titration calorimetry (ITC) experiments were performed for investigation of binary mixtures comprised of the Brønsted superbase DBN with hydrogen ethanoate (AcOH). The heat of mixing ($H^E$) profile was recorded at (343.15 ± 0.1) K and fitted with a 5-parameter Redlich-Kister (RK) polynomial. RK fit parameters were subsequently used to quantify partial molar heats of mixing, $x_i H_i^E$, for each component *i*. ITC-based complexometric titration data for the binary mixtures were recorded separately in methyl isobutyl ketone (mibk) and dodecane, to investigate the energetics of *non-random* clustering phenomena. Variable temperature $^1$H-NMR in combination with ATR-FTIR spectroscopic analyses were employed in parallel for elucidation and verification of liquid state ion speciation. These investigations reveal a strongly *non-ideal* system, and indicate "superbase" character of DBN is preserved for specific compositions where stoichiometric ionic liquids (ILs) form. Available ion speciation has been found to include $[DBN\text{-}H]^+$, $[AcO]^-$ as well as $\mu_2$-hydrogen-bridged, hydrogen-bonded *homoassociate* anions, of the type $[H(OAc)_2]^-$, with *double liquid salt* formation characterising various compositions based on spectroscopic determinations.



## 1. Introduction

In the past decade, superbase containing ionic liquids (ILs) have received significant attention towards their utility as solvents for biomass dissolution, in efforts to modernise the bioeconomy [1–4]. While the term "*superbase*" inspires notions of extremely strong basicity, analogous to the more established concept of "*superacid*", the definition developed hitherto is solely based upon structural features rather than on quantitative base strength (*e.g.* quantification *via* the well-known p$K_a$). To date, *aqueous* p$K_a$s have been determined for very few of these materials [5], and indicate favourable Gibbs energies of proton transfer, even from "weak" acids, which are on the order of –40 kJ mol$^{-1}$ (at 298.15 K) for a given acid-base pair. As p$K_a$s associated with Brønsted acidity are solvent dependent, *superbasicity* observed in aqueous mixtures provides no warranty for equivalent behaviour in *non-aqueous* environments such as those, for example, characterised as ILs [6], which prompted the interest for this experimental study.

In this investigation, binary mixtures of the superbase DBN with hydrogen ethanoate (AcOH) were examined in terms of the heat of mixing (excess enthalpy, $H^E$) profile, recorded at 343.15 ± 0.1 K, in order to quantify the extent the system is exothermically stabilised (*e.g.* by proton transfer from acid to base) across a large composition range, using the highly developed isothermal titration calorimetry (ITC) approach. In recent years, ITC has evolved from a technique employed mainly for thermodynamic determination of interactions between proteins and ligands [7–10], and for measurement of heat of mixing profiles [11], into one that can also be applied to investigate thermodynamics of other chemical interactions, such as Brønsted acid-base neutralisation reactions, and hydrogen-bonding phenomena [12–16]. Therefore, ITC was additionally employed to probe for the possibility of complex formation due to stabilising interactions between the superbase and hydrogen ethanoate.

Equimolar acid-base mixtures are known to form (usually) high melting temperature salts consisting of singly protonated conjugate acid $[DBN\text{-}H]^+$ cations with corresponding oppositely charged conjugate base $[AcO]^-$ anions, as has been reported previously based on NMR and X-ray crystallographic determinations [1,17].

* Corresponding Author.
*E-mail address:* gordon.driver@helsinki.fi (G.W. Driver).

https://doi.org/10.1016/j.jct.2021.106516
0021-9614/

Additional variable temperature $^1$H-NMR and ATR-FTIR analyses applied in this study reveal formation of Brønsted/Lewis conjugates previously undetected, where $\mu_2$-hydrogen-bridged, hydrogen-bonded diacetatohydrogenate(I), $[H(OAc)_2]^-$ type *homoassociate* anions are found to form *via* additional Brønsted/Lewis acid-conjugate base reactions. These findings are further supported by the experimental complexometric investigation presented here, which indicates complexation above the 1:1 composition.

## 2. Experimental

### 2.1. Materials

The superbase 1,5-diazabicyclo(4.3.0)non-5-ene, or, DBN, was purchased from Fluorochem with a stated mass fraction purity of 0.99 (molecular structure is presented in Scheme 1 below). The previously distilled base was again freshly distilled over BaO (to reactively remove $CO_2$ in the form of $Ba[CO_3]$, and $H_2O$ in the form of $Ba(OH)_2$), under inert conditions, with the distillate collected under Ar and stored in a sealed vessel. $^1$H-NMR analysis used to quantify the corresponding ring-opened hydrolysis product (HP-a) formed *via* chemical reaction with $H_2O$, revealed $x_{HP\text{-}a}$ = 0.006 ($x_{HP\text{-}a} \equiv$ mole fraction of HP-a) and a corresponding mass fraction of 0.007. Using the same method for the purification of DBN, m-TBD (7-methyl-1,5,7-triazabicyclo[4.4.0]dec-5-ene), synthesised in-house at the University of Helsinki, according to a recent patent [18], was found to contain $x_{HP\text{-}b}$ = 0.0001 ($x_{HP\text{-}b} \equiv$ mole fraction of HP-b, see Scheme 1) with an associated mass fraction of 0.0001[1] . Hydrogen ethanoate (*i.e.* acetic acid, AcOH) was purchased from Honeywell with a stated mass fraction purity of 0.998. Methyl isobutyl ketone (4-methylpentan-2-one or mibk, >0.997) and dodecane ($\geq$0.99), purchased from Sigma-Aldrich, were used as received. A materials summary is given in Table 1.

### 2.2. ITC

A TA-Instruments TAM III micro calorimeter was used for isothermal titration calorimetry (ITC) experiments. The apparatus was operated in dynamic correction mode at a thermostatted temperature set to (343.15 ± 0.1) K (uncertainty based on the manufacturer's precision specification for the set temperature). Two 4 mL cells were used as a sample cell and reference cell. The sample cell was stirred with a golden stirrer at a frequency of 1.33 $s^{-1}$. The amount of water in the reference cell was adjusted to ensure that this cell had in total an equal heat capacity to the average heat capacity of the sample cell.

Two types of ITC experiments were performed, *i.e.* measurement of the heat of mixing profile and measurement of the thermodynamic complexation data for acid-base complexation in other solvents. For the heat of mixing experiments, two separate titration experiments, *i.e.* titration of one component to the other and *vice versa*, together form one set of data. For the complexation measurements, the data set formed is based on a single titration experiment. The number of injections of each titration experiment was 24 and the injection volume was varied between 3 and 20 μL to improve data density on the most crucial parts of the curve. The injection interval was 1 h to ensure the signal returned to the baseline. To reduce effects resulting from the possibility of diffusive loss of titrant, a first injection of 3 μL was applied for each of the titrations. The associated data points resulting from these first injections were not further taken into account in the analysis. A standard deviation of < 5% in the heat released for reactions and interactions of this range was shown previously by Sprakel and Schuur [16].

Formation of the pure [DBN-H][$H(OAc)_2$] salt at $x_{DBN}$ = 0.333, followed by *double liquid salt* formation at $x_{DBN}$ = 0.375 (*i.e.* [DBN-H][AcO] + 2[DBN-H][$H(OAc)_2$]) and at $x_{DBN}$ = 0.427 (*i.e.* 2[DBN-H][AcO] + [DBN-H][$H(OAc)_2$]), and then by pure [DBN-H][AcO] formation at $x_{DBN}$ = 0.500, resulted in incrementally cumulative viscosity increases that forced the equipment into significant added power input for the stirrer. To exclude interference from the impact of compound formation and significantly increased viscosity with the measured heat effects, due to which correct interpretation of the pure heat of mixing effects from the titration results could be compromised, titrations for compositions in the range of $0.3 < x_{DBN} < 0.5$ were not performed for the final analysis (*c.f.* Fig. 1. and Table 3.).

### 2.3. Molecular modelling

Molecular modelling (MM) was performed with Wavefunction's Spartan'18 Parallel software to study complexes formed directly *via* interactions between acid and base molecules studied in this work. The initial geometry of DBN was obtained from a molecular mechanics simulation, with that of hydrogen ethanoate taken from the Spartan SSPD database. The molecular geometries for each individual species were then optimized by molecular modelling using the DFT-ωB97X-D-6-31G* level of theory, in combination with a parametrization to account for solvent polarity employing a conductor-like polarizable continuum solvation model (CPCM), using a default value of $\varepsilon_r$ = 37 to represent a high-dielectric medium. The geometry of the complex was subsequently optimized using the same level of theory. Energy profiles were calculated for the DBN + AcOH system, based on variation of constrained intermolecular distances. Absolute energy values reported were corrected using the calculated energy at large intermolecular distances for the complexes (>10 Å).

### 2.4. $^1$H-NMR

Proton spectra were acquired with a Bruker Avance NEO spectrometer (600 MHz $^1$H-frequency) equipped with a 5 mm triple resonance ($^1$H/$^{19}$F, $^{13}$C, $^{31}$P) inverse-detection probe-head, using a relaxation delay of 1 s and an acquisition time of 1.57 s. The sample was run neat with DMSO $d_6$ lock solvent contained in a sealed capillary immersed in the sample volume. The temperature unit was calibrated across a wide temperature range using a 4% methanol solution in methanol $d_4$, purchased from Sigma-Aldrich.

### 2.5. ATR-FTIR

Attenuated total reflection-Fourier transform infra-red (ATR-FTIR) spectra were recorded at room temperature using a Bruker Alpha instrument. Samples were run *neat* under ambient conditions with spectra recorded quickly to minimize possible uptake of atmospheric water and $CO_2$.

### 2.6. Modulated differential scanning calorimetry (MDSC)

A TA-Instruments Q200 DSC, calibrated using the In metal standard supplied with the instrument, was used in modulation mode to record melting temperatures reported in this work (below in Table 6). MDSC samples were measured in triplicate as a minimum either using separate sample pans, or, *via* separate experiments with the same sample pan, employing a modulation amplitude of ± 0.5 °C, a calibrated modulation period of 80 s, and a heating/-cooling rate of 3 °C $min.^{-1}$. For the samples investigated in this work, experiments were run with a total experiment time of

[1] $H_2O$ present is eliminated by reaction with TBD to form non-volatile hydrolysis products (that do not co-distill with the final product), during the methylation step *en route* to the synthesis and isolation of the final m-TBD product, see Reference 18.

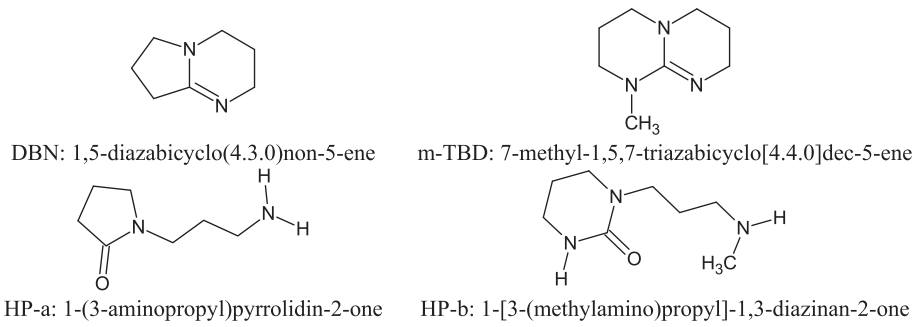


**Scheme 1.** Molecular structure of DBN, m-TBD and their corresponding hydrolysis products.

**Table 1**
Source and purity of materials.

| Chemical name | CAS RN® | Final mass fraction Purity | Method | Source |
|---|---|---|---|---|
| DBN[a] | 3001–72-7 | >0.99[b] | BaO, distillation | Fluorochem |
| m-TBD[a] | 84030–20-6 | >0.995[c] | BaO, distillation | University of Helsinki |
| mibk | 108–10-1 | >0.997[d] | | Sigma-Aldrich |
| Dodecane | 112–40-3 | ≥0.99[d] | | Sigma-Aldrich |
| Acetic acid | 64–19-7 | >0.991[e] | $^1$H-NMR analysis[f] | Honeywell |

[a] $H_2O$ is consumed *via* reaction of these bases into their hydrolysis products.
[b] In mass fraction (*via* analysis by $^1$H-NMR).
[c] In mass fraction (*via* analysis by $^1$H-NMR), and in accordance with the synthesis described in the patent [18].
[d] In mass fraction, as stated by the supplier.
[e] In mass fraction (*via* analysis by $^1$H-NMR).
[f] Details can be found in the supplementary information, *S1*.

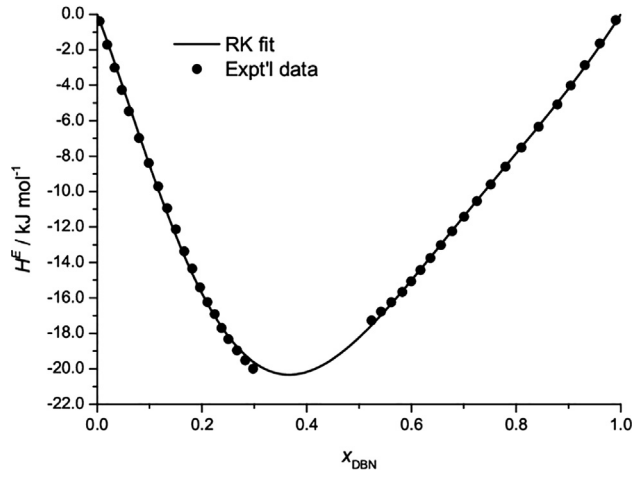


**Fig. 1.** $H^E$ profile recorded for DBN + AcOH at $T$ = (343.15 ± 0.1) K and $p$ = (100.7 ± 1.2) kPa. The extremum characterised by the RK fit is observed at $x_{DBN}$ = 0.368, with $H^E$ = −(20.3 ± 1.0) kJ mol$^{-1}$.

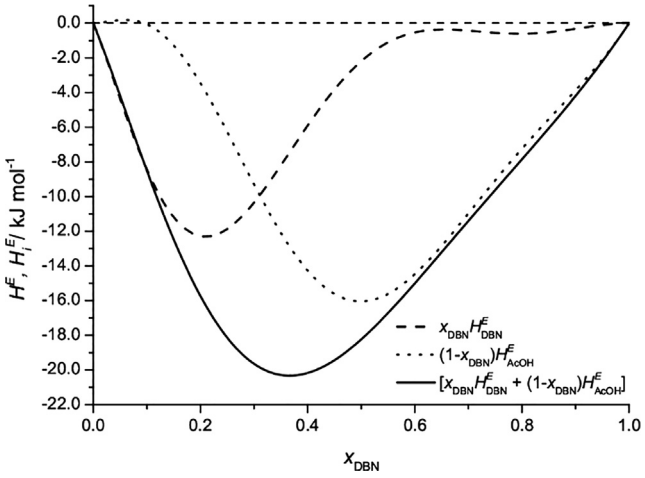


**Fig. 2.** Partial molar heats of mixing, $x_iH_i^E$, for each component $i$ in the DBN + AcOH system at (343.15 ± 0.1 K), calculated with RK parameters from Eq. (1) (shown below in Table 2), using Eqs. (2) and (3).

1112 min./experiment. A typical experiment employed 4 segments: a heating mode to 100 °C to remove thermal and mechanical history, a cooling mode to –80 °C, with an isothermal mode of several hours applied, followed by a final heating mode to 100 °C. MDSC signals other than those already identified as the melting endotherms relevant to this work will be discussed in a subsequent publication devoted to an in-depth phase diagram investigation.

## 3. Results

### 3.1. $H^E$ profile

The $H^E$ profile of the binary mixtures of DBN + AcOH, recorded at (343.15 ± 0.1) K, is given in Fig. 1, Fig. 2 presents partial molar contributions, $x_iH_i^E$, for each component $i$ of the binary system.

A 5-parameter Redlich-Kister (RK) polynomial, similar to a variant found in the literature [19], given in Eq. (1) below, was fitted to the $H^E$ data. Partial molar quantities ($x_iH_i^E$) were subsequently calculated using fit parameters obtained, according to Eqs. (2) and (3) ($x \equiv$ mole fraction DBN).

$$H^E_{RK}(x) = x(1-x)\left[\eta_1 + \eta_2(2x-1) + \eta_3(2x-1)^2 + \eta_4(2x-1)^3 + \eta_5(2x-1)^4\right] \quad (1)$$

$$H^E_{DBN}(x) = (1-x)^2[\eta_1 + \eta_2(4x-1) + \eta_3(2x-1)(6x-1) + \eta_4(2x-1)^2(8x-1) + \eta_5(2x-1)^3(10x-1)\Big] \quad (2)$$

**Table 2**
$H^E_{RK}$ best fit parameters obtained from data fitted using Eq. (1) for DBN + AcOH.

| System | $\eta_1$ | $\eta_2$ | $\eta_3$ | $\eta_4$ | $\eta_5$ |
|---|---|---|---|---|---|
| DBN + AcOH | −72.955 | 55.429 | −9.543 | −39.865 | 20.663 |

**Table 3**
Experimental and calculated heats of mixing in the binary system DBN + AcOH at $T$ = (343.15 ± 0.1) K and $p$ = (100.7 ± 1.2) kPa.

| | $H^E$/kJ mol$^{-1}$ | | | Eq. (2) | Eq. (3) |
|---|---|---|---|---|---|
| $x_{DBN}$ | Experimental | ±$U_c(H^E)$ | Eq. (1) | $x_{DBN}H^E_{DBN}$/kJ mol$^{-1}$ | $x_{AcOH}H^E_{AcOH}$/kJ mol$^{-1}$ |
| 0.005 | −0.382 | 0.025 | −0.349 | −0.353 | 0.003 |
| 0.019 | −1.71 | 0.09 | −1.53 | −1.58 | 0.05 |
| 0.033 | −3.01 | 0.15 | −2.73 | −2.84 | 0.11 |
| 0.047 | −4.26 | 0.21 | −3.92 | −4.09 | 0.16 |
| 0.061 | −5.47 | 0.27 | −5.09 | −5.28 | 0.19 |
| 0.080 | −6.97 | 0.35 | −6.79 | −6.91 | 0.13 |
| 0.099 | −8.39 | 0.42 | −8.38 | −8.33 | −0.05 |
| 0.116 | −9.71 | 0.49 | −9.87 | −9.52 | −0.35 |
| 0.134 | −10.9 | 0.6 | −11.2 | −10.5 | −0.77 |
| 0.150 | −12.1 | 0.6 | −12.5 | −11.2 | −1.29 |
| 0.166 | −13.4 | 0.7 | −13.6 | −11.7 | −1.89 |
| 0.181 | −14.3 | 0.7 | −14.6 | −12.1 | −2.55 |
| 0.196 | −15.4 | 0.8 | −15.5 | −12.3 | −3.26 |
| 0.210 | −16.2 | 0.8 | −16.3 | −12.3 | −4.01 |
| 0.224 | −16.9 | 0.9 | −17.0 | −12.3 | −4.77 |
| 0.238 | −17.7 | 0.9 | −17.6 | −12.1 | −5.54 |
| 0.250 | −18.3 | 0.9 | −18.2 | −11.9 | −6.30 |
| 0.267 | −19.0 | 0.9 | −18.8 | −11.5 | −7.30 |
| 0.283 | −19.5 | 1.0 | −19.2 | −11.0 | −8.25 |
| 0.298 | −20.0 | 1.0 | −19.6 | −10.4 | −9.16 |
| 0.524 | −17.3 | 0.9 | −17.5 | −1.60 | −15.9 |
| 0.542 | −16.8 | 0.8 | −17.0 | −1.24 | −15.7 |
| 0.562 | −16.2 | 0.8 | −16.3 | −0.93 | −15.4 |
| 0.583 | −15.7 | 0.8 | −15.6 | −0.68 | −14.9 |
| 0.599 | −15.1 | 0.8 | −15.0 | −0.54 | −14.5 |
| 0.617 | −14.4 | 0.7 | −14.4 | −0.44 | −14.0 |
| 0.636 | −13.7 | 0.7 | −13.7 | −0.38 | −13.3 |
| 0.656 | −13.0 | 0.7 | −13.0 | −0.36 | −12.6 |
| 0.678 | −12.2 | 0.6 | −12.2 | −0.38 | −11.8 |
| 0.701 | −11.4 | 0.6 | −11.4 | −0.43 | −11.0 |
| 0.725 | −10.5 | 0.5 | −10.5 | −0.49 | −10.0 |
| 0.751 | −9.60 | 0.48 | −9.57 | −0.56 | −9.01 |
| 0.780 | −8.59 | 0.43 | −8.57 | −0.60 | −7.97 |
| 0.810 | −7.51 | 0.38 | −7.49 | −0.60 | −6.89 |
| 0.843 | −6.34 | 0.32 | −6.31 | −0.55 | −5.77 |
| 0.879 | −5.09 | 0.25 | −5.01 | −0.42 | −4.59 |
| 0.904 | −4.01 | 0.20 | −4.04 | −0.30 | −3.73 |
| 0.931 | −2.87 | 0.14 | −2.97 | −0.18 | −2.79 |
| 0.960 | −1.64 | 0.08 | −1.78 | −0.07 | −1.71 |
| 0.990 | −0.320 | 0.022 | −0.437 | −0.004 | −0.433 |

$H^E \equiv$ excess enthalpy, $x_iH^E_i \equiv$ partial molar excess enthalpy for component $i \equiv$ DBN or AcOH, $x_{AcOH} = (1-x_{DBN})$. RK fit error: OF $=\sum_{k=0}^{40}\left(\frac{Expt'l-Calc'd}{Expt'l}\right)^2 = 0.185$, AAE% $=\sum_{k=0}^{40}\left|\frac{Expt'l-Calc'd}{Expt'l}\right|100 = 1.22$. Standard uncertainties $u$ (or $u_j$) are $u(x_{DBN}) = 0.006$, $u(p) = 1.2$ kPa, $u(T) = 0.1$ K, $u_j(H^E)$ values, calculated for a normal distribution, at the 0.99 confidence level using $k = 2.576$, are variable, and not worse than ± 0.4 kJ mol$^{-1}$ [16]. The combined expanded uncertainty, $U_c(H^E)$ was calculated at the 0.99 confidence level ($k = 2.576$).

$$H^E_{AcOH}(x) = x^2[\eta_1 + \eta_2(4x-3) + \eta_3(2x-1)(6x-5) + \eta_4(2x-1)^2(8x-7) + \eta_5(2x-1)^3(10x-9)] \quad (3)$$

Eq. (4) was employed as a consistency check.

$$H^E_{RK}(x) = xH^E_{DBN}(x) + (1-x)H^E_{AcOH}(x) \quad (4)$$

Fitted parameter values determined using Eq. (1) are presented in Table 2 below followed by the experimentally determined heat of mixing data, $H^E$, in Table 3.

### 3.2. Complexation curves and molecular modelling (MM)

Fig. 3 below gives the isotherm obtained from ITC measurement of complex formation of DBN with AcOH in mibk at (343.15 ± 0.1) K. With incremental increases in the mole ratio of AcOH over DBN, heats of injection were observed to decrease. The results were satisfactorily fitted with the 1:$n$ model, as has been applied previously by Sprakel and Schuur [15]. The relations for complexation reactions of $n$ molecules of *AcOH* with base *DBN*, and associated *K*-value resulting, are given in Eqs. (5) and (6), respectively, based on experimental data presented in Table 4, with resulting fit parameters presented in Table 5.

$$nAcOH + DBN \rightleftarrows AcOH_nDBN \quad (5)$$

$$K_{n,1} = \frac{[AcOH_nDBN]}{[nAcOH][DBN]} \quad (6)$$

The interaction energy profile of DBN with AcOH, calculated *via* MM, follows in Fig. 4.

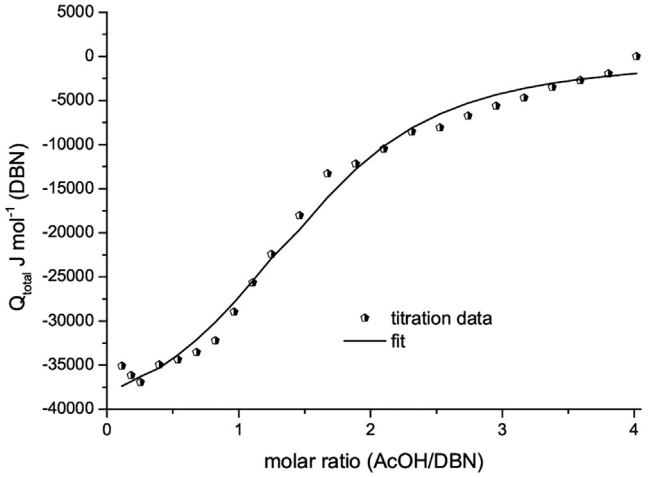


**Fig. 3.** Complexometric plot for DBN + AcOH in mibk at (343.15 ± 0.1) K: titration of pure AcOH to a 0.95 ± 0.01 mol dm$^{-3}$ solution of DBN ($x_{DBN}$ = 0.12) in mibk ($\varepsilon_r$ = 13.1 at 298.15 K [20]). (*cf.* Table 4). Experimental data fit error: OF = 0.0295, AAE% = 1.91.

**Table 4**
Heat of injection data comprising complexometric plot of DBN + AcOH in mibk at (343.15 ± 0.1) K and $p$ = (100.7 ± 1.2) kPa: titration of pure AcOH to a (0.95 ± 0.01) mol dm$^{-3}$ solution of DBN ($x_{DBN}$ = 0.12) in mibk. (*cf.* Fig. 3).[a]

| Mole ratio AcOH/DBN | $Q$ /kJ mol$^{-1}$ | $\pm U_c(Q)$ /kJ mol$^{-1}$ |
|---|---|---|
| 0.04 | −22.3[b] | 1.1 |
| 0.11 | −39.0 | 2.0 |
| 0.17 | −40.1 | 2.0 |
| 0.24 | −40.9 | 2.1 |
| 0.38 | −38.8 | 2.0 |
| 0.51 | −38.2 | 1.9 |
| 0.65 | −37.3 | 1.9 |
| 0.78 | −35.9 | 1.8 |
| 0.91 | −32.5 | 1.6 |
| 1.05 | −29.0 | 1.5 |
| 1.18 | −25.6 | 1.3 |
| 1.38 | −21.0 | 1.1 |
| 1.59 | −16.0 | 0.8 |
| 1.79 | −14.8 | 0.8 |
| 1.99 | −13.0 | 0.7 |
| 2.19 | −10.9 | 0.6 |
| 2.39 | −10.5 | 0.6 |
| 2.60 | −9.04 | 0.52 |
| 2.80 | −7.86 | 0.48 |
| 3.00 | −6.88 | 0.44 |
| 3.20 | −5.63 | 0.39 |
| 3.40 | −4.79 | 0.36 |
| 3.60 | −3.98 | 0.34 |
| 3.81 | −1.93 | 0.29 |

[a] Standard uncertainties $u$ (or $u_c$, or $u_j$) are $u(T)$ = 0.1 K, $u(p)$ = 1.2 kPa, $u_c$(AcOH/DBN) = 0.01, $u_j(Q)$ values, calculated for a normal distribution, at the 0.99 confidence level using $k$ = 2.576, are variable, and not worse than ± 0.8 kJ mol$^{-1}$ [15], and the combined expanded uncertainty $U_c(Q)$ was calculated at the 0.99 confidence level ($k$ = 2.576).

[b] This datum is an outlier presumably due to diffusion from the injection syringe upon initial equilibration.

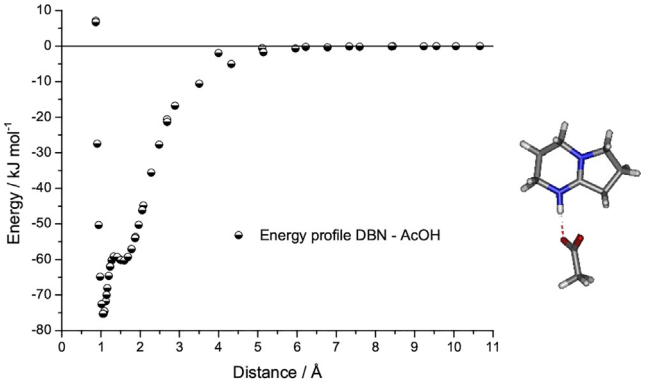


**Fig. 4.** Molecular modelling energy profile for DBN + AcOH over a range of intermolecular distances between the acidic proton of AcOH and the nitrogen atom of DBN using the DFT-$\omega$B97X-D-6-31G* level of theory with CPCM solvation employing the default value of $\varepsilon_r$ = 37.

### 3.3. Spectroscopic analyses

#### 3.3.1. $^1$H-NMR

Variable temperature (VT) $^1$H-NMR recording of spectra for the 3:5 DBN:AcOH system, presenting the decoalescence of the kinetic exchange averaged spectrum due to protons of [DBN-*H*]$^+$ and [AcO-*H*-OAc]$^-$, are given in Fig. 5 following. (for discussion see Section 4.2.1).

#### 3.3.2. ATR-FTIR

Room temperature ATR-FTIR spectra for various compositions of AcOH with DBN are given below in Fig. 6.

#### 3.3.3. Modulated differential scanning calorimetry (MDSC)

Melting temperature data required for discussion of salts and *double liquid salts*, included below in Section 4.2.3, are presented in Table 6 following.

## 4. Discussion

### 4.1. Heats of mixing, $H^E$

Binary mixtures of DBN with AcOH are highly *non-ideal* over the accessible composition range from pure base to pure acid, with the $H^E$ profile exhibiting an exothermic extremum as expected for mixtures expressing Brønsted acidity. In comparison to other bases, such as pyridine (Py) or aniline (An), regarded as *weak* in the aqueous milieu (p$K_a$ = 5.2 and p$K_a$ = 4.57, respectively), DBN appears to maintain its superior aqueous character accordingly in the *non-aqueous* mixtures, where use of the moniker "*superbase*" is justifiable. For example, the $H^E$ extremum in the Py + AcOH system reaches, at $x_{Py}$ = 0.41, a magnitude of –4.88 kJ mol$^{-1}$ at 298.15 K, and that in the system of An + AcOH, –4.67 kJ mol$^{-1}$, at $x_{An}$ = 0.32 [21]. By comparison, in the analogous title system, with DBN (aqueous p$K_a$ = 13.0 ± 1.5 [22]), at 343.15 ± 0.1 K, the $H^E$ extre-

**Table 5**
Complexation fit parameters for DBN + AcOH in mibk according to Eqs. (5) and (6), at $T$ = 343.15 ± 0.1 K. $K$ is the complexation equilibrium constant, $H$ the enthalpy of complexation associated with the Gibbs energy of complexation, $G$, and the entropy of complexation $S$. $G$ was obtained from $K$, and $S$ was subsequently computed from $G$ and $H$.

| System | solvent | $K$ | $H$/kJ mol$^{-1}$ | $G$/kJ mol$^{-1}$ | $S$/J K$^{-1}$ mol$^{-1}$ | $n$ |
|---|---|---|---|---|---|---|
| DBN-AcOH | mibk | 4.5 ± 0.5 | −43.8 ± 1.1 | −4.29 ± 0.3 | −115 ± 3 | 1.50 ± 0.03 |

$K \equiv$ complexation equilibrium constant, $H \equiv$ enthalpy of complexation, $G \equiv$ Gibbs energy of complexation, $S \equiv$ entropy of complexation. Relative standard uncertainty [15]: in $K$ ± 12% *(and related for this case in* $G$ ± 7.5% *and in* $S$ ± 3.0%*)*, in $H$ ± 2.5%, and in $n$ ± 1.6%.

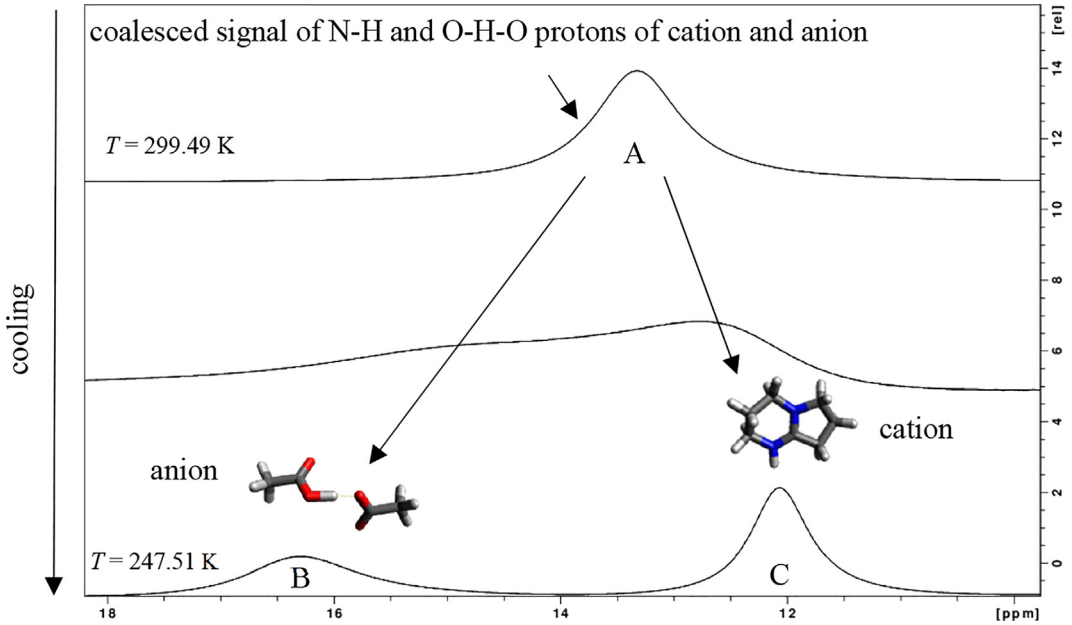


**Fig. 5.** VT-$^1$H-NMR spectra of DBN + AcOH ($x_{DBN}$ = 0.375) sample. Proton resonance A is due to coalescence of cationic N–$H^+$ and anionic O–$H$–O$^-$ resonances resultant from kinetic exchange of protons between [DBN-$H$]$^+$ and [AcO–$H$–OAc]$^-$. Proton resonance B is due to O–$H$–O$^-$ and resonance C to N–$H^+$ of the anion and cation, respectively.

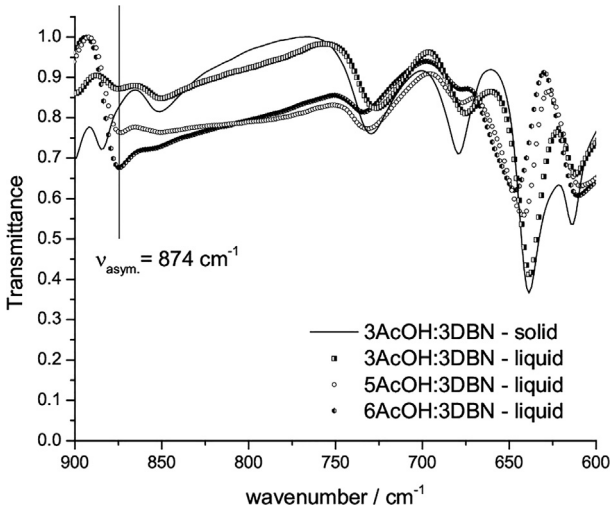


**Fig. 6.** Partial window ATR-FTIR spectra for various molar composition mixtures of DBN + AcOH. Evolution of the band at $\nu_{asym.}$ = 874 cm$^{-1}$ is due to the *homoassociate* diacetatohydrogenate(I) anion, [H(OAc)$_2$]$^-$.

mum is observed at $x_{DBN}$ = 0.368[2] with −(20.3 ± 1.0) kJ mol$^{-1}$. That the exothermic $H^E$ extremum of the DBN + AcOH system occurs at $x_{DBN}$ < 0.5 indicates, at least in enthalpic terms, the 1:1 binary salt composition of [DBN-H][AcO], is less stable than acid rich compositions in the range of $x_{DBN}$ > 0.3.

As the resulting RK fit was quite satisfactory (*cf.* Fig. 1, Section 3.1), fit parameters obtained were subsequently employed, *via* Eqs. (2) and (3), to quantify partial molar ($x_i H_i^E$) contributions according to each available component *i*, as was presented in Fig. 2. Consistency was checked using Eq. (4), giving satisfactory results. With a maximal partial molar contribution of $x_{DBN}H^E_{DBN}$ = −12.3 kJ mol$^{-1}$, it is clear that base strength in the *non-aqueous* mixtures appears to follow that observed in the aqueous environment. It is, however, AcOH that dominates the thermodynamics of mixing, and related chemistry in this system, with its maximal partial molar contribution of $(1-x_{DBN})H^E_{AcOH}$ = −16.0 kJ mol$^{-1}$ that clearly outweighs exothermal contributions to $H^E$ from DBN. This perhaps unexpected attribute is also observed with the Py + AcOH system, as is detailed later in the text (see Fig. 7 below).

Contributions to $H^E$ due to $(1-x_{DBN})H^E_{AcOH}$ are observed to be negative across all measured compositions in the region $x_{AcOH}$ = (1 − $x_{DBN}$) < 0.92 indicating for these mixtures with DBN, AcOH must, in the first instance, be present predominantly in monomeric form, since any initial breaking of hydrogen-bonded (AcOH)$_2$

[2] This value, provided by the RK fit, agrees well with the stoichiometric value of $x_{DBN}$ = 0.375, a composition which is characterised as a eutectic, exhibiting the lowest melting temperature observed in the 0.3 < $x_{DBN}$ < 0.5 mole fraction range.

**Table 6**
MDSC melting temperature data, $T_{mean}$, for selected compositions of DBN + AcOH and m-TBD + AcOH mixtures.[a]

| System | $x_{base}$[b] | Melting temperature[c] | |
|---|---|---|---|
| | | $T_{mean}$/K | ±$U_c(T_{mean})$/K |
| DBN + AcOH | 0.333 | 278.84 | 2.97 |
| | 0.375 | 274.29 | 1.92 |
| | 0.427 | 307.42 | 1.66 |
| | 0.500 | 334.68[d] | 1.75 |
| m-TBD + AcOH | 0.385 | 280.09 | 4.49 |
| | 0.500 | 350.34 | 4.13 |

[a] Recorded using a heating/cooling ramp of 3 °C min.$^{-1}$. Melting temperatures correspond to the liquidus line (the solid phase at the liquidus curve was not determined in this work). In all cases, the melting temperature was marked at the signal maximum, due to the broadness of the peaks. Example thermograms can be found in the supplementary information, *S2*.

[b] Samples were weighed into hermetic T-Zero aluminium pans and sealed; experimental pressure was not controlled beyond sealing the sample pans at $p$ = (100.7 ± 1.2) kPa.

[c] $T_{mean}$ ≡ mean melting temperature value. Standard uncertainties $u$ are $u(x_{DBN})$ = 0.006, $u(x_{m-TBD})$ = 0.006, $u(p)$ = 1.2 kPa, $u(T)$ = 0.05 K, $u$(scan-rate) = 0.002, $u(T_{mean})$ values are variable, and not worse than ± 1.7 K, and $U_c(T_{mean})$ is the combined expanded uncertainty at the 0.99 confidence level ($k$ = 2.576).

[d] Melting temperatures for the compound formed at this composition, *i.e.* [DBN-H][AcO], are reported over the range 315.1–320.9 K in Reference 3 due to use of the "onset" temperatures in characterisation of the resulting endotherms. For broadened signals, the "onset" approach becomes ill-defined, marking the melting temperature at the signal maximum is preferred for characterisation consistency.

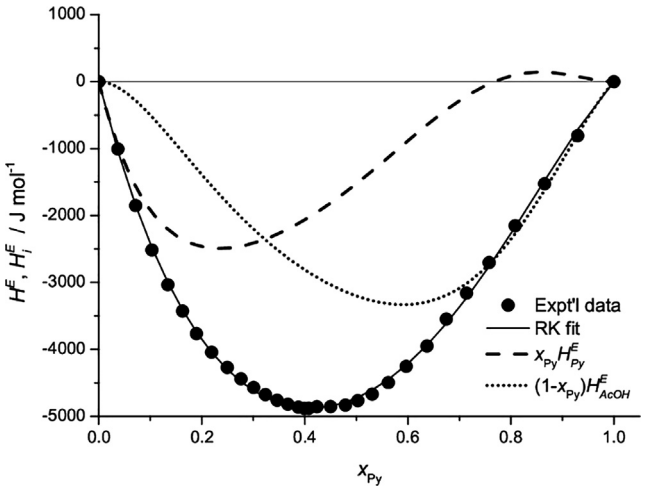


**Fig. 7.** Molar, $H^E$, and partial molar, $x_iH_i^E$ (for each component *i*), heats of mixing in the Py + AcOH system. Data were taken from [21,24], fitted using Eqs. (1)–(3), truncated to 4-parameters [19], and satisfactorily checked for consistency using Eq. (4) (Section 3.1).

dimers, as has been observed in the $H_2O$ + AcOH system [19], would be expected to make endothermic contributions to $H^E$ across a significant $x_{AcOH}$ range. Such lack of AcOH self-association strongly suggests these mixtures are highly polar as dimerisation constants, known to be inversely proportional to system polarity, take maximal values in apolar systems [23]. Additionally, formation of highly stabilised hydrogen-bonded *homoassociate* species, $[H(OAc)_2]^-$, *via* Brønsted/Lewis neutralisation of AcOH by available quantities of basic $[AcO]^-$, is indeed shown to occur by both $^1$H-NMR and ATR-FTIR (Section 4.2). These stabilised anionic species are expected to exothermically push $(1-x_{DBN})H^E_{AcOH}$ further down to more negative values, as a consequence of strongly exothermic hydrogen-bond bridge formation.

Interestingly, a similar analysis of the aforementioned Py + AcOH system, using a 4-parameter Redlich-Kister (RK) polynomial [19], revealed similar solution behaviour due to partial molar contributions from Py and AcOH, differing only in terms of the observation of an endothermic extremum at $x_{Py} > 0.76$ with a magnitude of $x_{Py}H^E_{Py} = +0.143$ kJ mol$^{-1}$, as presented in Fig. 7 below.

While the chemical basis of the composition dependent endothermal contributions of $x_{Py}H^E_{Py}$ to the overall $H^E$ is difficult to elucidate, the origin of such an effect may be found in compositionally dependent changes to overall system polarity, which are known to occur in other Brønsted acid-base conjugate mixtures containing carboxylates [25]. With *pure* liquid hydrogen ethanoate largely populated by strongly hydrogen-bonded, high-symmetry cyclic dimers, a low static relative dielectric permittivity ($\varepsilon_r$), with a weak temperature dependence, results. For example, at $T$ = 333.15 K, $\varepsilon_r$ = 6.5, a slight increase from $\varepsilon_r$ = 6.2 at room temperature (*i.e.* symmetric dimeric $(AcOH)_2$) is non-polar due to cancellation of dipole-moments) [26,27]. For Py-*rich* compositions exhibiting endothermic partial molar enthalpies of mixing, quantities of *homoassociate* anions $[H(OAc)_2]^-$ may already populate the liquid mixture. This type of charged *homoassociate* carboxylate anion is expected to contribute to large relative increases in $\varepsilon_r$ (*i.e.* up to $\Delta\varepsilon_r > 30$) due to structural character that results in the formation of a large dipole-moment, relative to the respective carboxylic monomer (or dimer) [28,29], as well as to the bases Py and $[AcO]^-$. While endothermic contributions due to DBN were not observed in its heat of mixing profile with AcOH, it is in any case also expected to contribute to a lesser degree towards overall system polarity, where, for example, structurally similar 1,1,3,3-tetramethylguanidine is found to possess $\varepsilon_r$ = 11.5 [30] , pyridine exhibits $\varepsilon_r$ = 13.26 [31].

### 4.2. Spectroscopic analyses

#### 4.2.1. Variable temperature $^1$H-NMR

In Fig. 5 from Section 3.3.1 above, VT-$^1$H-NMR spectra of DBN + AcOH ($x_{DBN}$ = 0.375) are presented. The averaged signal A ($\delta$ = 13.34 ppm) at 299.49 K contains contributions from both the nitrogenic proton of $[DBN\text{-}H]^+$ and the bridging proton of $[H(OAc)_2]^-$ due to fast proton exchange kinetics [32]. Cooling of the sample to 247.51 K reveals de-coalescence of signal A into signals B and C due to a drastic reduction of the proton exchange rate. Signal B ($\delta$ = 16.29 ppm) is due to the bridging proton of the $[AcO{-}H{-}OAc]^-$ *homoassociate* anion, and signal C ($\delta$ = 12.06 ppm) to the N–$H^+$ of the cation, with a population ratio of 1B:1.5C.

While synthesis of the 1:1 salt is known to produce distinct cations and anions, the solids, when melted, are capable of reforming free base. Concomitant quantities of free acid are thus liberated, which undergo further Brønsted/Lewis acid-base neutralisation reactions with available $[AcO]^-$ units to yield stable $\mu_2$-hydrogen-bridged [33][3], hydrogen-bonded *homoassociate* anions of the type $[HX_2]^-$, where X = $[AcO]^-$. The $^1$H-NMR spectrum at 247.51 K (*cf.* Fig. 5) reveals the presence of a hydrogen-bonded species with a characteristic low field resonance, exhibiting a chemical shift of $\delta$ = 16.29 ppm. Singly bonded protons typically exhibit isotropic chemical shifts in the range of < 13 ppm (*e.g.* nitrogenic protons), while those of strongly hydrogen-bonded species are expected at lower fields, in the vicinity of $\delta$ = ~15 ppm, as has been observed for the $\mu_2$-hydrogen-bridged proton presented in this work, and elsewhere [34,35]. Additionally, strongly hydrogen-bonded protons are expected to exhibit unusually large chemical shift anisotropies, $\Delta\sigma$, an NMR parameter that is very sensitive to hydrogen-bonding conditions, for which it is observed in the $\Delta\sigma$ > 30 ppm range [36]. Since such parameters were not experimentally available for this investigation, a high quality gas phase *in silico* computation for the geometric optimisation of $[H(OAc)_2]^-$ was performed using Gamess (version September 30, 2018 R3) at the MP2 6–311+G(d,p) level of theory utilising a vibrational analysis that ensured the resultant ionic geometry to be at the true energy minimum. The NMR shielding tensor was subsequently calculated for the optimised ionic geometry using the GIAO-B3LYP level of theory. Processing of the chemical shielding tensor pertaining to the $\mu_2$-hydrogen-bridged proton contained in $[H(OAc)_2]^-$ provided the *rank-2* traceless symmetric shielding tensor [37] which in turn revealed $\Delta\sigma$ = 38.56 pp m. The calculated isotropic chemical shift for the $\mu_2$-hydrogen-bridged proton (with ppm values relative to an averaged TMS value, calculated using the same *in silico* methods), due to the single *gas phase* anion (*i.e.* in the absence of shielding effects) gave a somewhat lower field value of $\delta$ = 20.03 ppm (in accord with the expected direction of the liquid-to-gas shift), comparing quite satisfactorily with condensed phase values reported above, in full support of the presence of $[H(OAc)_2]^-$.

#### 4.2.2. ATR-FTIR

ATR-FTIR spectra for various compositions of DBN + AcOH presented in Fig. 6 in Section 3.3.2 above indicate the evolution of a band at a wavenumber of 874 cm$^{-1}$, which intensifies proportionally with increases in the AcOH mole fraction (*i.e.* $(1 - x_{DBN})$), and which is absent only in the solid 1:1 binary salt composition. This band is characteristic of the asymmetric stretching mode ($\nu_{asym}$)

[3] The $\mu_2$- affix signifies that a group so designated bridges two centres of coordination, as given in Reference 33.

expected for the asymmetric O–H–O stretching frequency of *asymmetric* [AcO–H–OAc]$^-$ type anions [38,39]. In "glacial" hydrogen ethanoate, a similar band, characterising the O–H–O linkages of the symmetrical dimer, $(AcOH)_2$, appears at $\nu_{asym}$ = 935 cm$^{-1}$ [26,40]. The low magnitude wavenumber observed (*i.e.* < 1000 cm$^{-1}$) is indicative of a very strong hydrogen-bond [35,39], with $[H(OAc)_2]^-$ being characterised by a single-minimum asymmetric potential energy well across the linear $\mu_2$-hydrogen-bridged hydrogen-bond [39]. The ATR-FTIR analysis, therefore, aligns very well with the main structural conclusions determined *via* the VT-$^1$H-NMR analysis.

#### 4.2.3. Double liquid salts

At non-stoichiometric compositions, these mixtures of AcOH + DBN[‡] are capable of producing *double liquid salts* of the type $[cation][X]_{x_{base}}[Y]_{(1-x_{base})}$, whereby the common cation $[DBN\text{-}H]^+$ is paired with both $[AcO]^-$ and $[H(OAc)_2]^-$ anionic species. One particularly interesting composition, $x_{DBN}$ = 0.375, contains 3 DBN and 5 AcOH molar equivalents comprising the stoichiometric distillable *double liquid salt* $[DBN\text{-}H][AcO]_{0.33}[H(OAc)_2]_{0.67}$ (*e.g.* [DBN-H][AcO] + 2[DBN-H][$H(OAc)_2$]) [32,41], with $H^E$ = –(20.3 ± 1.0) kJ mol$^{-1}$ and a melting temperature of (274.29 ± 1.92) K. This material forms a negative azeotrope in the vapour state [32,41], similar to its behaviour with other carboxylates [42], and a stoichiometric eutectic in the liquid and solid states [32,41]. In a similar fashion, the 3:4 DBN:AcOH mole ratio mixture yields another *double liquid salt*, with a stoichiometry of $[DBN\text{-}H][AcO]_{0.67}[H(OAc)_2]_{0.33}$, at $x_{DBN}$ = 0.427 (*e.g.* 2[DBN-H][AcO] + [DBN-H][$H(OAc)_2$]), which exhibits $H^E$ = –(19.8 ± 1.0) kJ mol$^{-1}$, and melts at a temperature of (307.42 ± 1.66) K. The 3:3 composition consisting of [DBN-H][AcO] exhibits $H^E$ = –(18.2 ± 0.9) kJ mol$^{-1}$, with a melting temperature of (334.68 ± 1.75) K (at $x_{DBN}$ = 0.500), while the 3:6 composition, [DBN-H][$H(OAc)_2$] (with $x_{DBN}$ = 0.333) gives $H^E$ = –(20.2 ± 1.0) kJ mol$^{-1}$ and melts at a temperature of (278.84 ± 2.97) K [32,41].

Of additional interest here is the m-TBD analogue of $[DBN\text{-}H][AcO]_{0.33}[H(OAc)_2]_{0.67}$, a similar *non-stoichiometric* (*e.g.* [m-TBD-H][AcO] + 1.63[m-TBD-H][$H(OAc)_2$]) *double liquid salt*, and distillable *negative azeotrope* determined in this work to be comprised of $x_{m\text{-}TDB}$ = 0.385 [43][4] with a melting temperature of (280.09 ± 4.49) K [32]. Crystal platelet formation observed to occur in the $[m\text{-}TBD\text{-}H][AcO]_{0.38}[H(OAc)_2]_{0.62}$ liquid reveals precipitation of [m-TBD-H][AcO] (at $x_{m\text{-}TBD}$ = 0.500), with a melting temperature of (350.34 ± 4.13) K, from [m-TBD-H][$H(OAc)_2$] (at $x_{m\text{-}TBD}$ = 0.333), which remains as an ionic liquid "*mother-liquor*" (verified by $^1$H-NMR, spectra are available in the supplementary information, *S3*).

It is noteworthy that such *double liquid salts*, distillable or otherwise, can generally be expected to occur for any (base + carboxylate) system, regardless of base strength, with the possibility for volatile binary compositions located in the vicinity of exothermic extrema in the corresponding heat of mixing profile. For example, the much weaker base Py, with AcOH, exhibits negative azeotropy at $x_{Py}$ = 0.41, for the volatile *double liquid salt* non-stoichiometric mixture comprised of [Py-H][AcO] + 1.27[Py-H][$H(AcO)_2$], as $[Py\text{-}H][AcO]_{0.44}[H(OAc)_2]_{0.56}$, with $H^E$ = –4.88 kJ mol$^{-1}$ and a melting temperature of 222.15 K [41,44,45,46].

### 4.3. Complexation curves and molecular modelling

The centre point of the steeply sloped segment of the sinusoidal complexation curve, given in Fig. 3 (Section 3.2) which graphically presents interactions between AcOH and DBN in mibk, is not located at a mole ratio of 1, as would be expected for the case of complexation following a 1:1 stoichiometry. The centre point is instead located at a mole ratio of ~ 1.5, indicating formation of larger complexes composed of excess AcOH, with fitted values for the enthalpy of complexation indicating interactions between AcOH and DBN start to become exothermic (*cf.* Table 4). Additionally, when comparing the obtained isotherm to those typical of 1:*n* behaviour [9,15,16], it is clear that slopes larger than expected are visible at mole ratios ≥ 2, indicating formation of complexes containing multiple acid and base molecules. With similar measurements performed to probe interactions between DBN with AcOH using a relatively non-polar diluent, dodecane ($\varepsilon_r$ = 2.015 at 293.15 K [44]), a larger value for complex stoichiometries was obtained, *i.e.* $n$ = (1.63 ± 0.03), indicating formation of complexes that on average contain yet more AcOH molecules than with mibk as diluent. Such results are not entirely unexpected since AcOH is known to form open-chain (asymmetric) branched, uncharged- or charged-polymers in solutions [47], in a similar fashion to hydrogen halide varieties [48,49,50].

For interactions between DBN and AcOH, MM results presented in Fig. 4 (Section 3.2) indicate a clear and strong extremum at 1 Å, suggestive of proton transfer, with 1 Å representing a typical covalent bond distance for N–H bonds [44]. The 2nd extremum visible in the energy profile, observed at 1.7 Å, indicates strong, short-distance hydrogen-bonding, and is possibly representative of the equilibrium between hydrogen-bonding and full proton transfer, where only some fraction of hydrogen-bonds created result in full proton transfer [51,52].

## 5. Conclusions

The $H^E$ profile reveals binary mixtures of DBN with AcOH are exothermic and strongly *non-ideal*, with a deeply negative $H^E$ extremum observed, in far excess of the classical Brønsted reference bases, *e.g.* pyridine and aniline. A satisfactory RK fit of the $H^E$ profile provided entrance to determination of the corresponding partial molar contributions $x_i H_i^E$. It appears that AcOH plays a dual role in terms of heat evolution, where it has been observed to exothermically transfer protons not only to DBN, but also to $[AcO]^-$ conjugates, yielding highly stabilised diacetatohydrogenate(I) *homoassociate* anions, $[H(OAc)_2]^-$. AcOH is thereby observed to possess both Brønsted *and* Lewis acid-base character in the DBN system, as is expected in general terms for similar carboxylic acid–base systems.

Spectroscopic analyses presented here, using techniques chosen for their unique ability to probe hydrogen-bonding effects, reveal the presence of $\mu_2$-hydrogen-bridged hydrogen-bonded $[H(OAc)_2]^-$ anions in stable *double liquid salt* mixtures comprised of $x_{AcOH} > 0.50$, and may also be expected to occur in the fused 1:1 binary salt composition, as was revealed for [DBN-H][AcO] *via* the ATR-FTIR analysis. These *double liquid salts*, formalised as $[base\text{-}H][AcO]_{x_{base}}[H(OAc)_2]_{(1-x_{base})}$, appear to be unavoidable across 1/5 of the available mole fraction range, from $0.3 < x_{base} < 0.5$, with *non-random* clustering phenomena, observed in both mibk and dodecane, revealing the possibility for formation of higher order complexes in such *acid-rich* compositions.

All evidence presented in this work suggests qualitatively, and quantitatively (in terms of enthalpies), that DBN exhibits extremely strong basicity in mixtures with AcOH. Further support is similarly found in the complexometric data, in combination with the molecular modelling analysis. These clearly indicate the occurrence of strong exothermic interactions between hydrogen ethanoate and DBN. As a result, the moniker "*superbase*", which at this point in time has been quantitatively demonstrated for DBN only

[‡] $H^E$ values presented in this Section were calculated for the respective system using Eq. (1), Section 3.1. Mean melting temperature values, $T_{mean}$, stated with their associated $U_c$ values, are presented in Table 6, Section 3.3.3.

[4] Vapour pressure data for this azeotropic composition, reported as $x_{m\text{-}TBD}$ = 0.40 (*e.g.* [m-TBD-H][AcO] + 1.5[m-TBD-H][$H(OAc)_2$]), are available in Reference 43.

in aqueous solution, appears to be justified for use in the *non-aqueous* systems, according to the investigations presented here, even in the absence of quantitative p$K_a$ data. In the title system, however, as well as in those comprised of the weaker bases, AcOH dominates the thermodynamics of mixing, with its dual role Brønsted/Lewis acid-base chemistry. Exothermic contributions arising from $(1-x_{base})H^E_{AcOH}$, *via* protonation reactions with both DBN, and its own conjugate, $[AcO]^-$, to overall $H^E$, are proportionally larger than those originating, not only from DBN, but also from the other relatively weaker bases considered in this work, *i.e.* $(1-x_{base})H^E_{AcOH} \gg x_{base}H^E_{base}$.

## Declaration of Competing Interest

The authors declare that they have no known competing financial interests or personal relationships that could have appeared to influence the work reported in this paper.

## Acknowledgements

GWD and IK acknowledge The Bio-based Industries Joint Undertaking (BBI-ju) project GRETE (www.greteproject.eu), and LMJS and BS the Institute for Sustainable Process Technology (ISPT), for funding. Jussi Helminen (UH) is thanked for discussions regarding superbase hydrolysis and Sami Heikkinen (UH) for discussions regarding aspects of the NMR analysis.

## Appendix A. Supplementary data

Supplementary data to this article can be found online at https://doi.org/10.1016/j.jct.2021.106516.

## References

[1] A. Parviainen, R. Wahlström, U. Liimatainen, T. Liitiä, S. Rovio, J.K.J. Helminen, U. Hyväkkö, A.W.T. King, A. Suurnäkki, I. Kilpeläinen, RSC Adv. 5 (2015) 69728–69737.
[2] S. Elsayed, S. Hellsten, C. Guizani, J. Witos, M. Rissanen, A.H. Rantamäki, P. Varis, S.K. Wiedmer, H. Sixta, A.C.S. Sustain. Chem. Eng. (2020).
[3] A. Ostonen, J. Bervas, P. Uusi-Kyyny, V. Alopaeus, D.H. Zaitsau, V.N. Emelyanenko, C. Schick, A.W.T. King, J. Helminen, I. Kilpeläinen, A.A. Khachatrian, M.A. Varfolomeev, S.P. Verevkin, Ind. Eng. Chem. Res. 55 (2016) 10445–10454.
[4] G.W. Driver, I.A. Kilpeläinen, RSC Adv. 10 (2020) 42200–42203.
[5] K. Kaupmees, A. Trummal, I. Leito, Croat. Chem. Acta 87 (2014) 385–395.
[6] L.M. Mihichuk, G.W. Driver, K.E. Johnson, ChemPhysChem 12 (2011) 1622–1632.
[7] M. Kabiri, L.D. Unsworth, Biomacromolecules 15 (2014) 3463–3473.
[8] R.J. Falconer, J. Mol. Recognit. 29 (2016) 504–515.
[9] L. Damian, Methods Mol. Biol. (N. Y., NY, U. S.) 1008 (2013) 103–118.
[10] J.E. Ladbury, B.Z. Chowdhry, Chem. Biol. 3 (1996) 791–801.
[11] M.R. de Rivera, F. Socorro, J.S. Matos, Int. J. Mol. Sci. 10 (2009) 2911–2920.
[12] R. Cuypers, B. Burghoff, A.T.M. Marcelis, E.J.R. Sudhölter, A.B. de Haan, H. Zuilhof, J. Phys. Chem. A 112 (2008) 11714–11723.
[13] R. Cuypers, S. Murali, A.T.M. Marcelis, E.J.R. Sudhoelter, H. Zuilhof, ChemPhysChem 11 (2010) 3465–3473.
[14] R. Cuypers, E.J.R. Sudhoelter, H. Zuilhof, ChemPhysChem 11 (2010) 2230–2240.
[15] L.M.J. Sprakel, B. Schuur, Ind. Eng. Chem. Res. (2018) 12574–12582.
[16] L.M.J. Sprakel, B. Schuur, J. Ind. Eng. Chem. 72 (2019) 364–373.
[17] A. Parviainen, A.W.T. King, I. Mutikainen, M. Hummel, C. Selg, L.K.J. Hauru, H. Sixta, I. Kilpeläinen, ChemSusChem 6 (2013) 2161–2169.
[18] J. Helminen, A. King, I. Kilpeläinen, World Patent, WO 2019/092319 Al, (2018).
[19] A.N. Campbell, J.M.T.M. Gieskes, Can. J. Chem. 43 (1965) 1004–1011.
[20] M.D. Sacks, C.S. Khadilkar, J. Am. Ceram. Soc. 66 (1983) 488–494.
[21] H. Keidea, F. Herold, H.J. Rademacher, Z. Phys, Chem. 261O (1980) 809–812.
[22] Personal Communication: I. Leito, for the estimation of the pKa of DBN.
[23] Y. Fujii, H. Yamada, M. Mizuta, J. Phys. Chem. 92 (1988) 6768–6772.
[24] S.I. Sandler, Chemical, Biochemical, and Engineering Thermodynamics, 4th ed., John Wiley & Sons, 2006.
[25] F. Kohler, H. Atrops, H. Kalali, E. Liebermann, E. Wilhelm, F. Ratkovics, T. Salamon, J. Phys. Chem. 85 (1981) 2520–2524.
[26] J. Emsley, J. Chem. Soc. A (1971) 2702–2708.
[27] W. Dannhauser, R.H. Cole, J. Am. Chem. Soc. 74 (1952) 6105.
[28] Y.Y. Borowikow, Zh. Obshch, Khim. (1968) 1215–1219.
[29] P. Huyskens, N. Felix, A. Janssens, F. Van den Broeck, F. Kapuku, J. Phys. Chem. 84 (1980) 1387–1393.
[30] M.L. Anderson, R.N. Hammer, J. Chem. Eng. Data 12 (1967) 442–447.
[31] S. Malanowski, R. Patz, M.T. Rätzsch, C. Wohlfarth, Fluid Phase Equilib. 3 (1979) 291–312.
[32] G.W. Driver, unpublished results.
[33] IUPAC Compendium of Chemical Terminology Gold Book v. 2.3.3, 2014.
[34] J.H. Clark, J. Emsley, J. Chem. Soc., Dalton Trans. (1973) 2154–2159.
[35] P.E. Hansen, J. Spanget-Larsen, Molecules 22 (2017) 552–572.
[36] P. Schuster, W. Mikenda (Eds.), Hydrogen Bond Research, Springer-Verlag, Wien, 1999.
[37] J. Kowalewski, L. Mäler, Nuclear Spin Relaxation in Liquids: Theory, Experiments, and Applications, Taylor Francis, Boca Raton, 2006.
[38] A. Brbot-Šaranović, D. Hadži, M. Hodošček, B. Orel, J. Mol. Struct. 140 (1986) 269–279.
[39] T.A. O'Shea, Ph. D. Thesis, University of Warwick, 1969.
[40] E. Reyhanitash, E. Fufachev, K.D. van Munster, M.B.M. van Beek, L.M.J. Sprakel, C.N. Edelijn, B.M. Weckhuysen, S.R.A. Kersten, P.C.A. Bruijnincx, B. Schuur, Green Chem. 21 (2019) 2023–2034.
[41] G.W. Driver, Oral presentation at ILSEPT - 4th International Conference on Ionic Liquids in Separation and Purification Technology, 8-11 September 2019, Melia Sitges, Sitges, Spain.
[42] F.M.S. Ribeiro, C.F.R.A.C. Lima, A.M.S. Silva, L.M.N.B.F. Santos, ChemPhysChem 19 (2018) 2364–2369.
[43] Z.S. Baird, P. Uusi-Kyyny, J. Witos, A.H. Rantamäki, H. Sixta, S.K. Wiedmer, V. Alopaeus, J. Chem. Eng. Data 65 (2020) 2405–2421.
[44] D.R. Lide, CRC Handbook of Chemistry and Physics, 74th ed., CRC Press, Boca Raton, 1993.
[45] R.G. Treble, K.E. Johnson, E. Tosh, Can. J. Chem. 84 (2006) 915–924.
[46] K.E. Holmberg, Acta Chem. Scand. 13 (1959) 717–721.
[47] N.P. Aravindakshan, K.E. Gemmell, K.E. Johnson, A.L.L. East, J. Chem. Phys. 149 (2018) 094505.
[48] G.W. Driver, I. Mutikainen, Dalton Trans. 40 (2011) 10801–10803.
[49] G. Driver, K.E. Johnson, Green Chem. 5 (2003) 163–169.
[50] G. Driver, M.Sc. Thesis, The University of Regina, 2003.
[51] P. Gilli, L. Pretto, V. Bertolasi, G. Gilli, Acc. Chem. Res. 42 (2009) 33–44.
[52] L.I. Krishtalik, BBA-Bioenerg. 1458 (2000) 6–27.

JCT-D-20-00313